



## Synthesis, in vitro and in vivo evaluation of fluorine-18 labelled FE-GW405833 as a PET tracer for type 2 cannabinoid receptor imaging

Nele Evens<sup>a,†</sup>, Caroline Vandeputte<sup>b,c</sup>, Giulio G. Muccioli<sup>d,‡</sup>, Didier M. Lambert<sup>d</sup>, Veerle Baekelandt<sup>c</sup>, Alfons M. Verbruggen<sup>a</sup>, Zeger Debyser<sup>c</sup>, Koen Van Laere<sup>b</sup>, Guy M. Bormans<sup>a,\*</sup>

<sup>a</sup> Laboratory for Radiopharmacy, IMIR K.U. Leuven, O&N2, Herestraat 49, Bus 821, BE-3000 Leuven, Belgium

<sup>b</sup> Division of Nuclear Medicine, IMIR K.U. Leuven, Leuven, Belgium

<sup>c</sup> Molecular Medicine, IMIR K.U. Leuven, Leuven, Belgium

<sup>d</sup> Louvain Drug Research Institute, Medicinal Chemistry Group, UCLouvain, Bruxelles, Belgium

### ARTICLE INFO

#### Article history:

Received 10 May 2011

Revised 6 June 2011

Accepted 9 June 2011

Available online 16 June 2011

#### Keywords:

Type 2 cannabinoid receptor

MicroPET

[<sup>18</sup>F]FE-GW405833

Neuroinflammation

### ABSTRACT

The type 2 cannabinoid receptor (CB<sub>2</sub>R) is part of the endocannabinoid system and is expressed in tissues related to the immune system. As the CB<sub>2</sub>R has a very low brain expression in non-pathological conditions, but is upregulated in activated microglia, it is an interesting target for visualization of neuroinflammation using positron emission tomography with a suitable radiolabeled CB<sub>2</sub>R ligand. In this study, we radiolabelled a fluoroethyl derivative of GW405833, a well known CB<sub>2</sub>R partial agonist, with fluorine-18 (half-life 109.8 min) by alkylation of the phenol precursor with 1-bromo-2-[<sup>18</sup>F]fluoroethane. In vitro studies showed that FE-GW405833 behaved as a selective high affinity (27 nM) inverse agonist for hCB<sub>2</sub>R. [<sup>18</sup>F]FE-GW405833 showed moderate initial brain uptake in mice and rats, but a slow washout from brain and plasma due to retention of a radiometabolite. Specific binding of the tracer to human CB<sub>2</sub>R was demonstrated in vivo in a rat model with local CB<sub>2</sub>R overexpression in the brain. Optimized derivatives of GW405833 that are less susceptible to metabolism will need to be developed in order to provide a useful tracer for CB<sub>2</sub>R quantification with PET.

© 2011 Elsevier Ltd. All rights reserved.

### 1. Introduction

The type 1 (CB<sub>1</sub>R) and type 2 (CB<sub>2</sub>R) cannabinoid receptor and probably also GPR55 are receptors of the endocannabinoid system, which also consists of endogenous ligands, such as anandamide and 2-arachidonoyl glycerol, and proteins for their biosynthesis, and degradation.

The CB<sub>1</sub>R has been the center of attention for several years and hence its function is better studied compared to CB<sub>2</sub>R. CB<sub>1</sub>R is mainly expressed in the central nervous system and several PET radioligands have been developed to investigate this receptor allowing elucidation of its role in neuropsychiatric disorders, eating disorders and drug dependence.<sup>1</sup>

The CB<sub>2</sub>R is involved in the immune system, and expression has been shown in spleen, lymph nodes and Peyer's patches.<sup>2</sup> In the periphery, upregulation of CB<sub>2</sub>R expression has been observed in

atherosclerotic plaques and in endometrial inflammation.<sup>3,4</sup> Although CB<sub>2</sub>R was initially considered to be the peripheral cannabinoid receptor, it is now well accepted that CB<sub>2</sub>R are expressed on activated microglia and macrophages in brain.<sup>5,6</sup> Although CB<sub>2</sub>R expression on neurons remains controversial<sup>7</sup> a role of CB<sub>2</sub>R has also been attributed to neurologic pathologies such as depression,<sup>8</sup> eating disorders<sup>9</sup> and drug abuse.<sup>10</sup>

CB<sub>2</sub>R upregulation linked to neuroinflammation is observed in the brain of Alzheimer patients where activated microglia cluster at  $\beta$ -amyloid plaques.<sup>11,12</sup> Fernandez-Ruiz and co-workers described upregulation of CB<sub>2</sub>R in the striatum of a rat chronic lesion model of Huntington's disease (HD) and both hypoxia-ischemia and middle cerebral artery occlusion induced the expression of CB<sub>2</sub>R-positive microglia in rat brain.<sup>13,14</sup> Moreover, the spinal cord of a mouse model of amyotrophic lateral sclerosis (ALS) and plaques of demyelination in multiple sclerosis patients showed an increase in CB<sub>2</sub>R.<sup>15,16</sup>

Hence, a CB<sub>2</sub>R PET tracer can be a valuable research tool to explore the role and importance of CB<sub>2</sub>R in (neuro)inflammation and to evaluate the therapeutic value of new CB<sub>2</sub>R-related drugs.

GW405833 (L-768,242) is a well known CB<sub>2</sub>R selective agonist.<sup>17</sup> Several studies describe its anti-inflammatory, anti-nociceptive and anti-hyperalgesic actions in animal models of neuropathic and inflammatory pain.<sup>18,19</sup> Indeed, besides analgesia, GW405833 also

\* Corresponding author. Tel.: +32 16330447; fax: +32 16330449.

E-mail addresses: [Evensnele@gmail.com](mailto:Evensnele@gmail.com) (N. Evens), [guy.bormans@pharm.kuleuven.be](mailto:guy.bormans@pharm.kuleuven.be) (G.M. Bormans).

<sup>†</sup> O&N2, Herestraat 49, Bus 821, BE-3000 Leuven, Belgium. Tel.: +32 16330441; fax: +32 16330449.

<sup>‡</sup> Present address: Bioanalysis and Pharmacology of Bioactive Lipids laboratory, CHAM7230, Université Catholique de Louvain, Bruxelles, Belgium.

has inhibitory effects on gliosis in a rat neuropathic pain model.<sup>20</sup> As CB<sub>2</sub>R agonists seem to act not only at non-neuronal sites but also at neuronal level, they are proposed as being an interesting target for the treatment of chronic pain.<sup>21</sup> However, Schuelert and co-workers described increased nociceptor activity in an osteoarthritic knee joint rat model when treated with GW405833, but decreased joint nociception in control animals.<sup>22</sup>

Recently, the development of several carbon-11 labelled PET radioligands with CB<sub>2</sub>R affinity were reported.<sup>23–25</sup> Horti et al. provided proof of principle for CB<sub>2</sub>R imaging in pathological conditions with a neuroinflammatory component.<sup>25</sup>

Due to its longer half-life (~110 min), radiolabelling with fluorine-18 allows to inject multiple subjects from the same production batch and provides an opportunity to transport the tracer to remote sites. Our group described the development of a fluorine-18 labelled CB<sub>2</sub>R selective 2-oxoquinoline derivative, that suffered from major drawbacks such as a low radiochemical yield, a high bone uptake and a relatively low affinity compared to its carbon-11 labelled counterpart.<sup>26</sup> We recently reported carbon-11 radiolabeled GW405833 that in combination with an adeno-associated viral vector encoding for an inactive mutant of human CB<sub>2</sub>R (hCB<sub>2</sub>R(D80N)) was evaluated as a PET reporter gene system for brain.<sup>27</sup>

In this study, we have synthesized and evaluated fluorine-18 labelled GW405833 as a PET tracer for the in vivo visualization of CB<sub>2</sub>R.

## 2. Results and discussion

### 2.1. Synthesis and radiosynthesis

The phenol precursor **1** ((2,3-dichlorophenyl)-[5-hydroxy-2-methyl-3-(2-morpholin-4-yl-ethyl)-indol-1-yl]-methanone) was synthesized by demethylation of GW405833 with BBr<sub>3</sub>. Alkylation of **1** with 1-bromo-2-fluoroethane in the presence of potassium carbonate as a base provided authentic FE-GW405833 in 40% yield.

[<sup>18</sup>F]FE-GW405833 was obtained by alkylation of **1** with 1-bromo-2-[<sup>18</sup>F]fluoroethane in the presence of Cs<sub>2</sub>CO<sub>3</sub> with a decay corrected radiochemical yield of 33 ± 6%, a radiochemical purity >95% (n = 5) and a specific activity of 50–100 GBq/μmol (Fig. 1). The overall preparation time including the synthesis of 1-bromo-2-[<sup>18</sup>F]fluoroethane was 70 min.

### 2.2. Log D and affinity

The log D of [<sup>18</sup>F]FE-GW405833 was determined by partitioning between 1-octanol and 0.025 M phosphate buffer pH 7.4 and was found to be 2.8. The calculated polar surface area (cPSA) was 43.7 Å<sup>28</sup>. These values are almost identical to those observed for GW405833<sup>27</sup> and are within the ideal range for blood–brain barrier (BBB) penetration. Indeed, favourable molecular characteristics for entering the brain are a low molecular mass (<600 Da), a cPSA less than 90 Å<sup>2</sup> and a log partition coefficient between 1 and 3.

The affinity of FE-GW405833 for the human CB<sub>2</sub>R (hCB<sub>2</sub>R) and human CB<sub>1</sub>R (hCB<sub>1</sub>R) was determined in a competition binding assay. The affinity of FE-GW405833 for hCB<sub>1</sub>R was ~10 μM and 27 nM for hCB<sub>2</sub>R. This affinity value is comparable to that described for GW405833.<sup>19</sup> As the B<sub>max</sub> of hCB<sub>2</sub>R in neuroinflammatory conditions is not known it is difficult to predict whether the affinity is high enough for sensitive detection of neuroinflammation. FE-GW405833 behaved as an inverse agonist in a [<sup>35</sup>S]-GTPγS assay with EC<sub>50</sub> = 17.9 nM and E<sub>max</sub> = –82%, values that are close to those observed for GW405833 in the same assay. GW405833 has been characterized both as a partial agonist and as an inverse agonist depending on the assay that was used.<sup>19,29</sup> Mancini and co-workers reported the inverse agonistic behaviour of GW405833 in a cAMP assay turning to agonistic behaviour when the receptor constitutive activity was abolished. GW405833 and its fluoroethyl derivative can thus be defined as a protean agonists, that is, partial agonists that produce a lower intrinsic efficacy than the naturally occurring constitutively active state, thereby effectively lowering

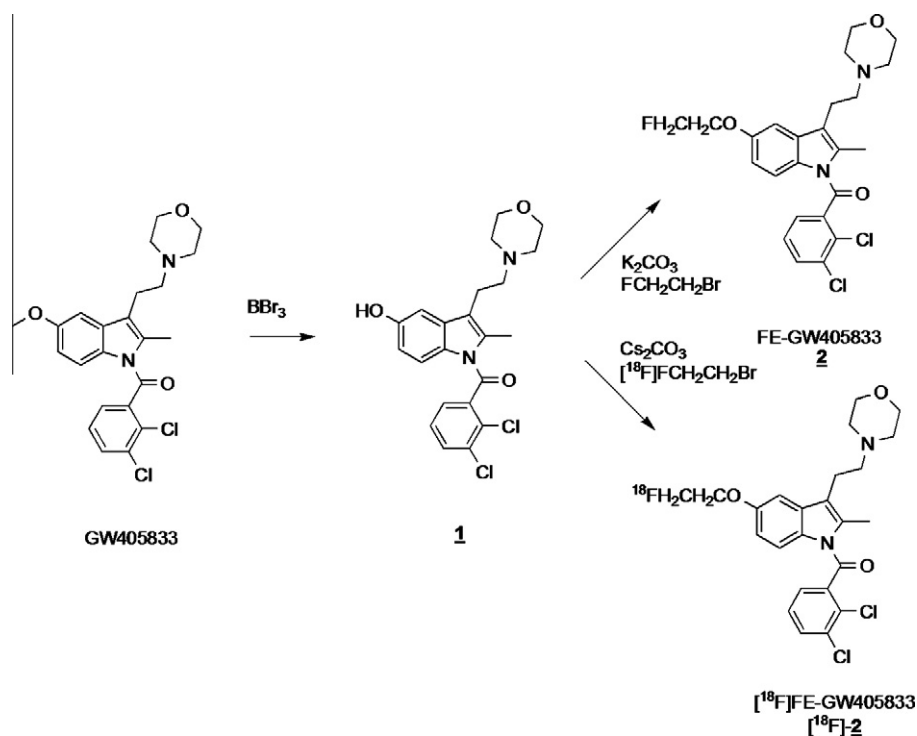


Figure 1. Radiosynthesis of [<sup>18</sup>F]FE-GW405833.

**Table 1**  
Biodistribution of [<sup>18</sup>F]FE-GW405833 in normal NMRI mice

Organ	% ID ± SD <sup>†</sup>		% ID/g ± SD <sup>‡</sup>		SUV ± SD <sup>#</sup>	
	2 min	60 min	2 min	60 min	2 min	60 min
Kidneys	9.8 ± 1.5	2.2 ± 0.5	15.8 ± 0.7	3.4 ± 0.7	5.5 ± 0.4	1.2 ± 0.2
Urine	0.1 ± 0.0	1.4 ± 0.5	—	—	—	—
Liver	47.4 ± 5.1	23.7 ± 3.2	26.3 ± 2.7	11.4 ± 0.8	9.1 ± 1.1	4.0 ± 0.4
Spleen	0.9 ± 0.2	0.3 ± 0.0	9.5 ± 0.8	3.1 ± 0.6	3.3 ± 0.4	1.1 ± 0.2
Pancreas	0.7 ± 0.2	0.5 ± 0.4	3.6 ± 0.5	2.4 ± 1.5	1.2 ± 0.2	0.8 ± 0.6
Lungs	3.4 ± 0.1	0.7 ± 0.1	13.1 ± 2.1	2.4 ± 0.5	4.5 ± 0.7	0.8 ± 0.2
Heart	1.1 ± 0.1	0.3 ± 0.1	7.7 ± 0.9	2.1 ± 0.4	2.7 ± 0.2	0.7 ± 0.1
Intestines	8.9 ± 1.2	35.7 ± 4.7	—	—	—	—
Stomach	1.3 ± 0.3	1.8 ± 1.0	—	—	—	—
Blood	4.5 ± 0.4	5.0 ± 1.0	1.9 ± 0.2	2.1 ± 0.5	0.6 ± 0.1	0.7 ± 0.2
Brain	1.3 ± 0.1	0.7 ± 0.1	2.9 ± 0.1	1.6 ± 0.3	1.0 ± 0.1	0.6 ± 0.1

Data are expressed as mean ± SD; n = 4 per time point.

<sup>†</sup> Percentage of injected dose calculated as cpm in organ/total cpm recovered.

<sup>‡</sup> Percentage of the injected dose per gram tissue.

<sup>#</sup> Standard uptake values calculated as (radioactivity in cpm in organ/weight of the organ in g)/(total counts recovered/body weight in g).

the receptor activity, giving the impression of inverse agonistic behavior.<sup>30</sup>

### 2.3. Ex vivo and in vivo experiments

The biodistribution of [<sup>18</sup>F]FE-GW405833 was studied in mice at 2 and 60 min post injection (p.i.) (Table 1). A predominant hepatobiliary excretion was observed with a high uptake in the liver at 2 min post injection (p.i.) (47% ID) and a significant excretion to the intestines (36% ID at 60 min pi). Blood concentration remained constant between 2 and 60 min p.i. probably due to the generation of a radiometabolite with long plasma half-life. Brain uptake of [<sup>18</sup>F]FE-GW405833 was moderate with a value 1.3% ID at 2 min p.i. Washout of the tracer was rather slow with still 0.7% ID being present at 60 min p.i. None of the studied peripheral organs showed significant retention of the tracer. The spleen, being the organ with the highest endogenous CB<sub>2</sub>R expression, would be the most likely organ to display CB<sub>2</sub>R tracer retention. The affinity of the tracer may be insufficient to visualize the limited endogenous splenic CB<sub>2</sub> receptor expression. Interspecies difference with regard to CB<sub>2</sub>R binding affinity between rodent and human CB<sub>2</sub>R is not likely as GW405833 was tested on CB<sub>2</sub>R in rat spleen homogenates and human CB<sub>2</sub>R expressing cells and showed a comparable affinity.<sup>19</sup>

Plasma radiometabolite analysis showed fast metabolism with only 12% of intact tracer left at 30 min p.i. (Fig. 2). Also in brain, the fraction of radiometabolites increased as a function of time p.i. with only 50% of intact tracer in brain at 30 min p.i. Brain retention of this radiometabolite is probably resulting in slow brain washout and may preclude CB<sub>2</sub>R quantification.

[<sup>18</sup>F]FECNT, a radioligand with high affinity for the dopamine transporter, shows in vivo dealkylation with formation of [<sup>18</sup>F]fluoroacetaldehyde and its oxidation product [<sup>18</sup>F]fluoroacetic acid. These radiometabolites were found to cross the BBB and to distribute uniformly throughout the brain.<sup>31</sup> The same radiometabolites may be generated by O-dealkylation of [<sup>18</sup>F]FE-GW405833, thus resulting in retention of radiometabolites in brain.

Although plasma clearance of [<sup>11</sup>C]-GW405833 was also slow, brain clearance was much faster with only 0.1% of ID in brain at 60 min p.i.<sup>27</sup> whereas initial brain uptake was comparable to that observed for [<sup>18</sup>F]FE-GW405833. For [<sup>11</sup>C]-GW405833, a comparable fraction of radiometabolites was found in plasma but no radiometabolites were found in brain.<sup>27</sup> This suggests that both tracers are metabolized by O-dealkylation but that only in the case of [<sup>18</sup>F]FE-GW405833 BBB permeable radiometabolites are generated.

A microPET study was performed to evaluate in vivo hCB<sub>2</sub>R binding specificity of [<sup>18</sup>F]FE-GW405833 in a rat model with local hCB<sub>2</sub>R overexpression.<sup>27</sup> hCB<sub>2</sub>R was overexpressed in the right striatum after stereotactic injection of an adeno-associated viral (AAV) vector encoding eGFP-T2A-hCB<sub>2</sub>R(D80N) (Fig. 3).

The microPET images showed absence of retention of activity in the skull suggesting that [<sup>18</sup>F]FE-GW405833 is not defluorinated.

The time activity curve (TAC) over the left striatum showed an initial peak and slow clearance up to about 60 min after which the activity level remained constant in agreement with the biodistribution data in mice.

The TAC over the right striatum showed a similar pattern but with a slower clearance resulting in a factor 1.6 higher concentration than the contralateral striatum at 60 min p.i., a ratio comparable to that observed for [<sup>11</sup>C]-GW405833.<sup>27</sup>

Since a control vector was injected in the contralateral hemisphere and since the microPET scan was performed 34 days after stereotactic surgery, potential unilateral uptake of the tracer due to BBB disruption is unlikely. The activity in the left striatum was comparable to the cerebellum level (control level). CB<sub>2</sub>R overexpression in the right striatum was confirmed by immunofluorescent staining for CB<sub>2</sub>R and eGFP, which demonstrated colocalization of both proteins (Fig. 3). Minor expression of CB<sub>2</sub>R was also detected in CD68<sup>+</sup> activated microglia and macrophages.

### 3. Conclusions

[<sup>18</sup>F]FE-GW405833 was evaluated as a CB<sub>2</sub>R radioligand and displayed high in vitro CB<sub>2</sub>R binding affinity and selectivity over CB<sub>1</sub>R, moderate brain uptake in mice and in vivo binding to the hCB<sub>2</sub>R. However, the presence of large fraction of radiometabolites in brain hampers its use for neuroinflammation imaging, a feature that may be shared by other [<sup>18</sup>F]fluoroethoxyphenyl compounds. Although GW405833 is a promising lead compound for development of a fluorine-18 CB<sub>2</sub>R PET tracer, other radiolabeled GW405833 derivatives that are less susceptible to generate radiometabolites that cross the BBB will need to be developed.

### 4. Materials and methods

#### 4.1. General conditions

For ascending thin layer chromatography, pre-coated aluminium backed plates (Silica Gel 60 with fluorescence indicator, 0.2 mm thickness; supplied by Macherey-Nagel, Düren, Germany)

were used and developed using mixtures of dichloromethane and methanol or hexane and ethylacetate as mobile phase. After evaporation of the solvent, compounds were detected under UV light (254 nm). High performance liquid chromatography (HPLC) analysis was performed using a system of a Merck-Hitachi L-7100 gradient pump (Merck, Darmstadt, Germany) connected to a UV-spectrometer (Merck-Hitachi L-4250 UV-VIS detector, Merck) set at 254 nm. Data were acquired and analyzed using RaChel (Lablogic, Sheffield, UK) or GINA Star (Raytest, Straubenhardt, Germany) data acquisition systems.

Molecular mass measurement was performed on a time-of-flight mass spectrometer (LCT, Micromass, Manchester, UK) equipped with an orthogonal electrospray ionization (ESI) interface. Acquisition and processing of data was done using Masslynx software (version 3.5, Micromass).

$^1\text{H}$  NMR spectra were recorded on a Bruker AVANCE 300 MHz spectrometer (Bruker AG, Faellanden, Switzerland) using  $\text{CDCl}_3$  or  $\text{DMSO}-d_6$  as solvent. The standard Bruker Topspin 1.3 software under Windows XP was used. Chemical shifts are reported in parts per million relative to tetramethylsilane ( $\delta = 0$ ). Coupling constants are reported in Hertz. Splitting patterns are defined by s (singlet), d (doublet), dd (double doublet), t (triplet), q (quadruplet), quint (quintet), sext (sextet) or m (multiplet).

## 4.2. Synthesis

### 4.2.1. 1-(2,3-Dichlorobenzoyl)-5-methoxy-2-methyl-3-[2-(4-morpholinyl)ethyl]-1H-indole (GW405833)

Synthesis of GW405833 was performed according to literature methods yielding a yellow solid (yield = 61%).  $^{19}\text{TLC}$ :  $R_f = 0.6$  (dichloromethane with 3%  $\text{CH}_3\text{OH}$ ) or  $R_f = 0.8$  (dichloromethane with 5%  $\text{CH}_3\text{OH}$ ). HPLC (XBridge RP18 column 5  $\mu\text{m}$ , 4.6 mm  $\times$  150 mm, Waters;  $\text{EtOH}/\text{NH}_4\text{OAc}$  0.05 M pH 6.9 60/40; 1 ml/min):  $t_R = 5.4$  min (99%).  $^1\text{H}$  NMR ( $\text{DMSO}$ )  $\delta$  7.899 (1H, d,  $^3J_{\text{H-H}} = 8.0$  Hz, 4- $\text{H}_{\text{ar}}$ ), 7.704 (1H, d,  $^3J_{\text{H-H}} = 7.0$  Hz, 6- $\text{H}_{\text{ar}}$ ), 7.587 (1H, t,  $^3J_{\text{H-H}} = 7.8$  Hz, 5- $\text{H}_{\text{ar}}$ ), 7.365 (1H, d,  $^3J_{\text{H-H}} = 8.5$  Hz, 7-H), 7.031 (1H, d,  $^4J_{\text{H-H}} = 2.3$  Hz, 4-H), 6.791 (1H, dd,  $^3J_{\text{H-H}} = 9.0$  Hz and  $^4J_{\text{H-H}} = 2.3$  Hz, 6-H), 3.796 (3H, s,  $\text{OCH}_3$ ), 3.574 (4H, t,  $^3J_{\text{H-H}} = 4.4$  Hz,  $2 \times \text{NCH}_2\text{CH}_2\text{O}$ ), 2.766 (2H, t,  $^3J_{\text{H-H}} = 7.6$  Hz,  $\text{CH}_2\text{CH}_2\text{N}$ ), 2.445–2.406 (6H, m,  $\text{CH}_2\text{CH}_2\text{N}$  and  $2 \times \text{NCH}_2\text{CH}_2\text{O}$ ), 2.014 (3H, s, 2- $\text{CH}_3$ ).

### 4.2.2. 1-(2,3-Dichlorobenzoyl)-5-hydroxy-2-methyl-3-[2-(4-morpholinyl)ethyl]-1H-indole (precursor for labelling, **1**)

To a stirred solution of GW405833 (0.320 g, 0.715 mmol) in dry dichloromethane (10 ml) under nitrogen at  $-70^\circ\text{C}$  a 1 M solution of boron tribromide in dichloromethane (2.9 ml) was added dropwise over 30–45 min. The mixture was maintained at  $-70^\circ\text{C}$  for

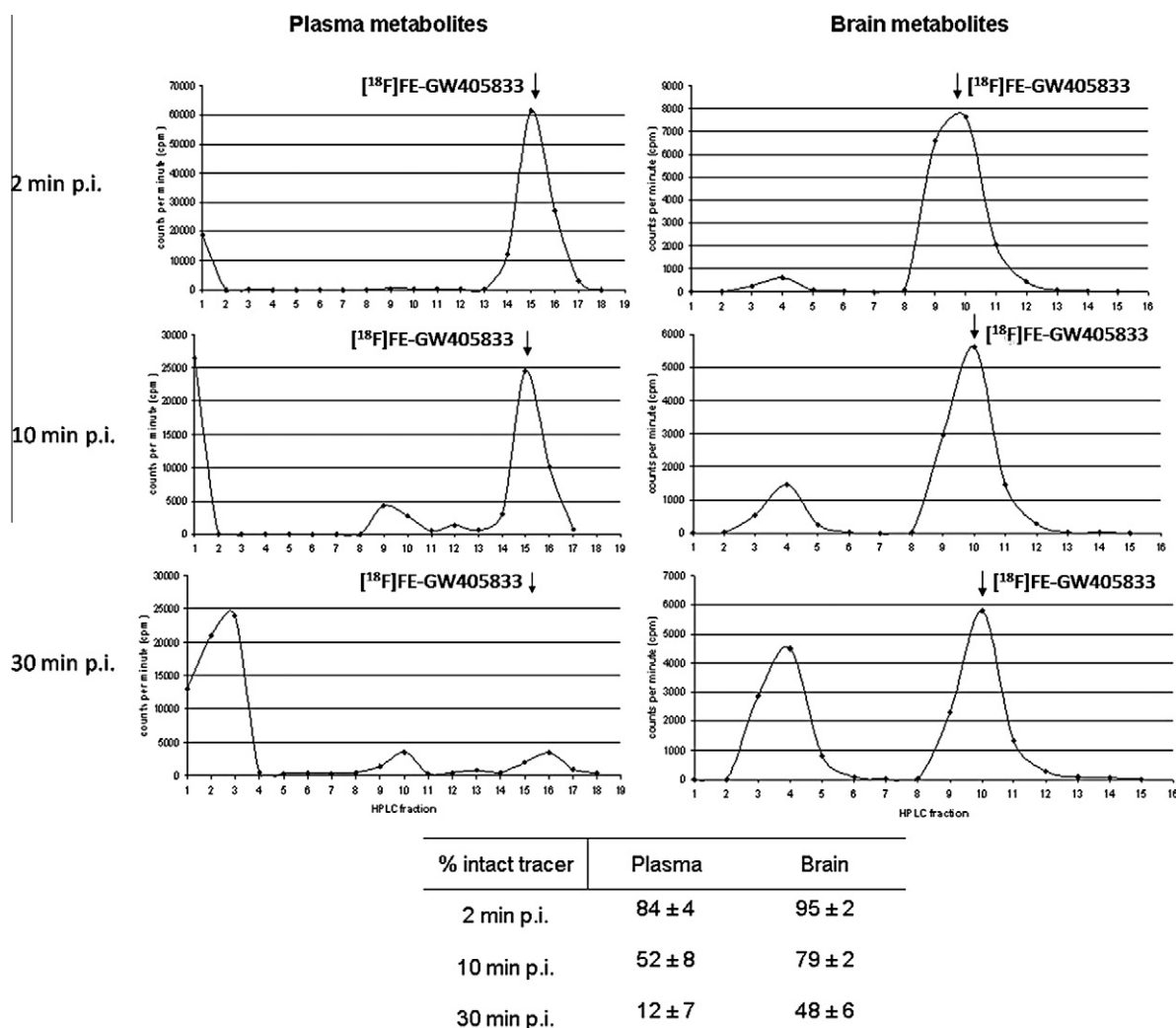


**Figure 2.** Plasma and brain radiometabolites of  $[^{18}\text{F}]\text{FE-GW405833}$  in normal NMRI mice 2, 10 or 30 min after tracer injection. HPLC analysis shows the percentage of intact tracer.

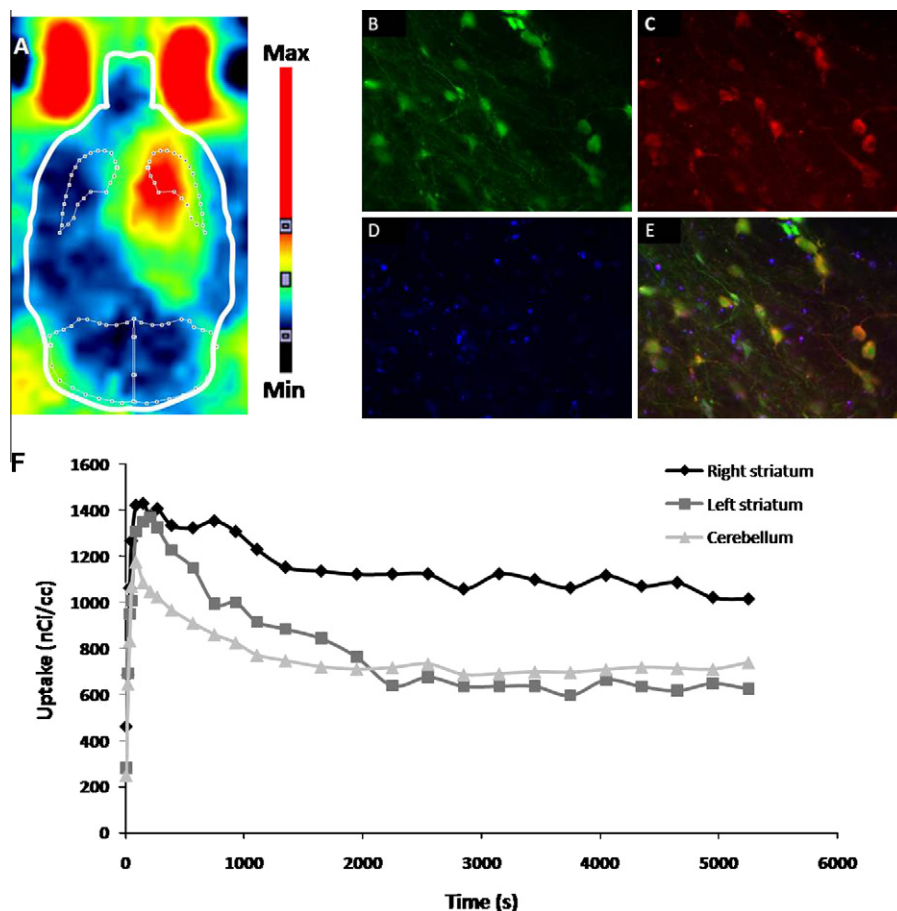


**Figure 3.** (A) Summed image of 30–90 min post injection of [ $^{18}\text{F}$ ]FE-GW405833 in a rat model with hCB $_2$ R overexpression in the right striatum. A control vector encoding eGFP was injected in the contralateral hemisphere. Triple immunofluorescent staining for (B) eGFP (FITC), (C) CB $_2$ R (647 nm), (D) CD68 $^+$  activated microglia and macrophages (Alexa 555 nm) and (E) an overlay image of the same rat. Colocalization of both eGFP and CB $_2$ R was observed in the right striatum. (F) Corresponding time-activity curve of [ $^{18}\text{F}$ ]FE-GW405833 in left and right striatum and cerebellum at 34 days after stereotactic surgery. Activity in the right striatum was on average twice as high compared to the contralateral hemisphere. The uptake in the latter was comparable to the uptake in the cerebellum.

1 h and then allowed to warm slowly to room temperature at which it was stirred overnight. The reaction mixture was again cooled to  $-70\text{ }^\circ\text{C}$  and the excess of boron tribromide was quenched by dropwise addition of methanol until no further reaction occurred. The reaction mixture was purified by column chromatography on silica gel (63–200  $\mu\text{m}$  particle size, 60  $\text{\AA}$ , MPBiomedicals, Eschwege, Germany) using dichloromethane–methanol (gradient 0–5% methanol) as the eluent yielding a yellow-white solid (0.192 g, yield = 62%). TLC:  $R_f = 0.6$  (dichloromethane with 5%  $\text{CH}_3\text{OH}$ ). HPLC (XTerra RP18 column 5  $\mu\text{m}$ , 4.6 mm  $\times$  250 mm, Waters;  $\text{CH}_3\text{CN}/\text{NH}_4\text{OAc}$  0.05 M pH 6.9 60/40; 1 ml/min):  $t_R = 6.1$  min (98%)  $^1\text{H}$  NMR (DMSO)  $\delta$  9.315 (1H, s, 5-OH), 7.881 (1H, dd,  $^3J_{\text{H-H}} = 8.0$  Hz and  $^4J_{\text{H-H}} = 1.4$  Hz, 4-H $_{\text{ar}}$ ), 7.672 (1H, dd,  $^3J_{\text{H-H}} = 7.6$  Hz and  $^4J_{\text{H-H}} = 1.4$  Hz, 6-H $_{\text{ar}}$ ), 7.567 (1H, t,  $^3J_{\text{H-H}} = 7.8$  Hz, 5-H $_{\text{ar}}$ ), 7.325 (1H, d,  $^3J_{\text{H-H}} = 8.1$  Hz, 7-H), 6.833 (1H, d,  $^4J_{\text{H-H}} = 2.3$  Hz, 4-H), 6.622 (1H, dd,  $^3J_{\text{H-H}} = 8.9$  Hz and  $^4J_{\text{H-H}} = 2.3$  Hz, 6-H), 3.575 (4H, t,  $2 \times \text{NCH}_2\text{CH}_2\text{O}$ ), 2.700 (2H, t,  $\text{CH}_2\text{CH}_2\text{N}$ ), 2.434–2.365 (6H, m,  $\text{CH}_2\text{CH}_2\text{N}$  and  $2 \times \text{NCH}_2\text{CH}_2\text{O}$ ), 1.966 (3H, s, 2- $\text{CH}_3$ ). MS (ES) $^+$  Accurate mass: [ $\text{C}_{22}\text{H}_{22}\text{Cl}_2\text{N}_2\text{O}_3 + \text{H}$ ] $^+$  theoretical mass 433.1080 Da and found 433.1070 Da.

#### 4.2.3. 1-(2,3-Dichlorobenzoyl)-5-(2-fluoroethoxy)-2-methyl-3-[2-(4-morpholinyl)ethyl]-1H-indole (reference product, FE-GW405833)

To a solution of **1** (0.050 g, 0.115 mmol) in dimethylformamide (10 ml) potassium carbonate (0.032 g, 0.230 mmol) and 1-bromo-2-fluoroethane (0.022 g, 0.173 mmol) were added and the reaction

mixture was stirred for 5 h at  $90\text{ }^\circ\text{C}$ . Water was added (10 ml) and the reaction mixture was extracted with dichloromethane ( $3 \times 20$  ml), the collected dichloromethane fractions were washed with water (30 ml) and brine (30 ml), and dried over  $\text{MgSO}_4$ . The excess solvent was evaporated and purification was done by silica gel column chromatography using a heptane/dichloromethane gradient (100:0–50:50) yielding FE-GW405833 as a white solid (0.022 g, 40%). TLC:  $R_f = 0.1$  (hexane/EtOAc 5/95) or  $R_f = 0.7$  (dichloromethane with 5%  $\text{CH}_3\text{OH}$ ). HPLC (XTerra RP18 column 5  $\mu\text{m}$ , 4.6 mm  $\times$  250 mm, Waters;  $\text{CH}_3\text{CN}$  (A)/ $\text{NH}_4\text{OAc}$  0.05 M pH 6.9 (B) linear gradient from 95% B to 5% B in 20 min, 5% B 5 min; 1 ml/min):  $t_R = 21.2$  min (99%).  $^1\text{H}$  NMR ( $\text{CDCl}_3$ )  $\delta$  7.657–7.625 (1H, m, 4-H $_{\text{ar}}$ ), 7.375–7.355 (3H, m, 7-H/5-H $_{\text{ar}}$ /6-H $_{\text{ar}}$ ), 6.977 (1H, d,  $^4J_{\text{H-H}} = 2.3$  Hz, 4-H), 6.769 (1H, dd,  $^3J_{\text{H-H}} = 9.0$  Hz and  $^4J_{\text{H-H}} = 2.4$  Hz, 6-H), 4.767 (2H, dt,  $^2J_{\text{H-F}} = 47.4$  Hz,  $^3J_{\text{H-H}} = 4.1$  Hz,  $\text{OCH}_2\text{CH}_2\text{F}$ ), 4.255 (2H, dt,  $^2J_{\text{H-F}} = 27.8$  Hz,  $^3J_{\text{H-H}} = 4.1$  Hz,  $\text{OCH}_2\text{CH}_2\text{F}$ ), 3.751 (4H, t,  $^3J_{\text{H-F}} = 4.5$  Hz,  $2 \times \text{NCH}_2\text{CH}_2\text{O}$ ), 2.803 (2H, t,  $^3J_{\text{H-H}} = 8.1$  Hz,  $\text{CH}_2\text{CH}_2\text{N}$ ), 2.541–2.486 (6H, m,  $\text{CH}_2\text{CH}_2\text{N}$  and  $2 \times \text{NCH}_2\text{CH}_2\text{O}$ ), 2.146 (3H, s, 2- $\text{CH}_3$ ). MS (ES) $^+$  Accurate mass: [ $\text{C}_{24}\text{H}_{25}\text{Cl}_2\text{FN}_2\text{O}_3 + \text{H}$ ] $^+$  theoretical mass 479.1299 Da and found 479.1286 Da.

### 4.3. Radiosynthesis

#### 4.3.1. Synthesis of 1-bromo-2-[ $^{18}\text{F}$ ]fluoroethane and [ $^{18}\text{F}$ ]FE-GW405833

1-Bromo-2-[ $^{18}\text{F}$ ]fluoroethane was synthesized according to methods described by Chitneni et al.<sup>32</sup> 1-Bromo-2-[ $^{18}\text{F}$ ]fluoroethane

was distilled with a stream of helium and passed through an ascarite column (6 mm × 150 mm) in a reaction vial containing 200 µg **1** and 2–4 mg Cs<sub>2</sub>CO<sub>3</sub> in 200 µl DMF. The reaction mixture was heated at 90 °C for 2 min, diluted with 1.8 ml ammonium acetate buffer 0.05 M pH 6.9 containing 30% ethanol and injected onto an XBridge RP18 column (5 µm, 4.6 mm × 150 mm; Waters) which was eluted with 0.05 M ammonium acetate buffer (pH 6.9)/EtOH (65:35 v/v, 1 ml/min), *t<sub>R</sub>* = 11.5 min.

#### 4.3.2. Quality control

Quality control for [<sup>18</sup>F]FE-GW405833 using authentic FE-GW405833 as a reference was done by HPLC on an XTerra RP18 column (5 µm, 4.6 mm × 250 mm, Waters) eluted with 0.05 M ammonium acetate buffer pH 6.9/acetonitrile (40:60 v/v, 1 ml/min), *t<sub>R</sub>* = 9.9 min.

#### 4.4. Competition binding assay and [<sup>35</sup>S]-GTPγS assay

The competition binding assay and [<sup>35</sup>S]-GTPγS assay were done according to previously described methods.<sup>33</sup>

#### 4.5. Octanol-buffer distribution coefficient

Determination of the distribution coefficient of [<sup>18</sup>F]FE-GW405833 by partitioning between 1-octanol and 0.025 M phosphate buffer pH 7.4 was done according to previously described methods.<sup>32</sup>

#### 4.6. Biodistribution studies

All animal experiments were carried out in compliance with the national laws relating to the conduct of animal experimentation and approved by the local Animal Ethics Committee. All biodistribution studies were conducted in male NMRI mice (37–50 g). Mice were anesthetized with isoflurane (2% in oxygen). The solution of the HPLC purified product was diluted with saline to a concentration of approximately 6 MBq/ml. An aliquot of 100 µl was injected via a tail vein. The animals were sacrificed by decapitation and the organs and body parts were dissected and weighed. The activity in the dissected organs and blood was measured using a gamma counter. For calculation of total blood radioactivity, blood mass was assumed to be 7% of the body mass.<sup>34</sup>

#### 4.7. Plasma and brain metabolites

Radiometabolites were quantified in plasma and brain of male NMRI mice according to previously described methods.<sup>26,35</sup> Plasma analysis was performed on an Oasis® HLB column (Hydrophilic–Lipophilic Balanced; 4.6 mm × 20 mm, Waters) connected to an analytical XTerra RP18 column (5 µm, 4.6 mm × 250 mm; Waters) eluted using 0.05 M ammonium acetate pH 6.9/acetonitrile (30/70 v/v, 1 ml/min). Brain samples were analyzed on an HPLC system which consisted of an XTerra™ RP18 column (5 µm, 4.6 mm × 250 mm; Waters) and ammonium acetate buffer 0.05 M pH 6.9/acetonitrile 40/60 (v/v) as mobile phase (1 ml/min).

#### 4.8. µPET study in a rat model with local hCB<sub>2</sub>R overexpression

An AAV vector (AAV2/7-eGFP-T2A-hCB<sub>2</sub>R(D80N)) encoding hCB<sub>2</sub>R with a point mutation (Asp80Asn or D80N) and enhanced green fluorescent protein (eGFP) was stereotactically injected in the right striatum (relative to Bregma: anteroposterior (AP) 0 mm, lateral (LAT) –2.8 mm and dorsoventral (DV) –5.5 mm to –4.5 mm) of a normal 8-week old Fisher rat, while a control eGFP vector was injected in the left striatum (AP 0 mm, LAT 2.8 mm and DV –5.5 mm to –4.5 mm).<sup>27,36</sup> A µPET scan was performed on day

34 after stereotactic injection of the vector. Prior to small animal PET imaging, rats were anesthetized using 3% isoflurane in 2.0 L/min oxygen. A dynamic acquisition was started immediately after IV injection of approximately 37 MBq of the tracer. For each subject, images were spatially normalized to a stereotactic space and analyzed using a predefined volume-of-interest approach (VOI). The procedure of spatial normalization and its validation have been described previously.<sup>37</sup>

#### 4.9. Histology

The rat was sacrificed with an intraperitoneal injection of pentobarbital followed by a transcardial perfusion with 4% paraformaldehyde in PBS. After removal of the brain and overnight postfixation, 50 µm coronal sections were made using a vibratome (Microm, Walldorf, Germany). For immunofluorescent staining, floating sections were washed and incubated overnight with antibodies raised against eGFP (chicken, 1:1000, Aves Labs, Tigard, Oregon, USA), CB<sub>2</sub>R (rabbit, 1:1000, Cayman Chemical) and CD68 (mouse, 1:2000, Chemicon, Millipore, Brussels, Belgium) in 10% donkey serum. After washing, the sections were incubated for 2 h with fluorescently labeled donkey anti-chicken antibody (FITC, Jackson Immunoresearch 1:400), donkey anti-mouse (Alexa 555 nm, Invitrogen, merelbeke, Belgium, 1:500) and donkey anti-rabbit (647 nm, Invitrogen, merelbeke, Belgium, 1:500). Finally the cell nuclei were stained with 4',6-diamidino-2-phenylindole (DAPI). Immunofluorescence analysis was done with the AXIO Imager Z1 of Zeiss (Zaventem, Belgium).

#### Acknowledgments

This research is funded by FWO-Vlaanderen grant G0775.10N and a Ph.D. grant of the Institute for the Promotion of Innovation through Science and Technology in Flanders (IWT-Vlaanderen). We thank Peter Vermaelen and Ann Van Santvoort for their skillful help with the animal experiments.

#### References

- Horti, A. G.; Van Laere, K. *Curr. Pharm. Des.* **2008**, *14*, 3363.
- Lynn, A. B.; Herkenham, M. *J. Pharmacol. Exp. Ther.* **1994**, *268*, 1612.
- Iuvone, T.; De Filippis, D.; Di Spiezo Sardo, A.; D'Amico, A.; Simonetti, S.; Sparice, S.; Esposito, G.; Bifulco, G.; Insabato, L.; Nappi, C.; Guida, M. *J. Cell. Mol. Med.* **2008**, *12*, 661.
- Steffens, S.; Veillard, N. R.; Arnaud, C.; Pelli, G.; Burger, F.; Staub, C.; Karsak, M.; Zimmer, A.; Frossard, J. L.; Mach, F. *Nature* **2005**, *434*, 782.
- Carlisle, S. J.; Marciano-Cabral, F.; Staab, A.; Ludwick, C.; Cabral, G. A. *Int. Immunopharmacol.* **2002**, *2*, 69.
- Maresz, K.; Carrier, E. J.; Ponomarev, E. D.; Hillard, C. J.; Dittel, B. N. *J. Neurochem.* **2005**, *95*, 437.
- Atwood, B. K.; Mackie, K. *Br. J. Pharmacol.* **2010**, *160*, 467.
- Garcia-Gutierrez, M. S.; Perez-Ortiz, J. M.; Gutierrez-Adan, A.; Manzanares, J. *Br. J. Pharmacol.* **2010**, *160*, 1773.
- Ishiguro, H.; Carpio, O.; Horiuchi, Y.; Shu, A.; Higuchi, S.; Schanz, N.; Benno, R.; Arinami, T.; Onaivi, E. S. *Synapse* **2009**, *64*, 92.
- Onaivi, E. S.; Ishiguro, H.; Gong, J. P.; Patel, S.; Meozzi, P. A.; Myers, L.; Perchuk, A.; Mora, Z.; Tagliaferro, P. A.; Gardner, E.; Brusco, A.; Akinshola, B. E.; Hope, B.; Lujilde, J.; Inada, T.; Iwasaki, S.; Macharia, D.; Teasensfitz, L.; Arinami, T.; Uhl, G. R. *PLoS ONE* **2008**, *3*, e1640.
- Ashton, J. C.; Glass, M. *Curr. Neuropharmacol.* **2007**, *5*, 73.
- Ramirez, B. G.; Blazquez, C.; Gomez del Pulgar, T.; Guzman, M.; de Ceballos, M. L. *J. Neurosci.* **2005**, *25*, 1904.
- Fernandez-Ruiz, J.; Romero, J.; Velasco, G.; Tolon, R. M.; Ramos, J. A.; Guzman, M. *Trends Pharmacol. Sci.* **2007**, *28*, 39.
- Ashton, J. C.; Rahman, R. M.; Nair, S. M.; Sutherland, B. A.; Glass, M.; Appleton, I. *Neurosci. Lett.* **2007**, *412*, 114.
- Shoemaker, J. L.; Seely, K. A.; Reed, R. L.; Crow, J. P.; Prather, P. L. *J. Neurochem.* **2007**, *101*, 87.
- Benito, C.; Romero, J. P.; Tolon, R. M.; Clemente, D.; Docagne, F.; Hillard, C. J.; Guaza, C.; Romero, J. *J. Neurosci.* **2007**, *27*, 2396.
- Gallant, M.; Dufresne, C.; Gareau, Y.; Guay, D.; Leblanc, Y.; Prasit, P.; Rochette, C.; Sawyer, N.; Slipetz, D. M.; Tremblay, N.; Metters, K. M.; Labelle, M. *Bioorg. Med. Chem. Lett.* **1996**, *6*, 2263.
- Hu, B.; Doods, H.; Treede, R. D.; Ceci, A. *Pain* **2009**, *143*, 206.

19. Valenzano, K. J.; Tafesse, L.; Lee, G.; Harrison, J. E.; Boulet, J. M.; Gottshall, S. L.; Mark, L.; Pearson, M. S.; Miller, W.; Shan, S.; Rabadi, L.; Rotshteyn, Y.; Chaffer, S. M.; Turchin, P. I.; Elsemore, D. A.; Toth, M.; Koetzner, L.; Whiteside, G. T. *Neuropharmacology* **2005**, *48*, 658.
20. Leichsenring, A.; Andriske, M.; Backer, I.; Stichel, C. C.; Lubbert, H. *Naunyn-Schmiedeberg's Arch. Pharmacol.* **2009**, *379*, 627.
21. Beltramo, M.; Bernardini, N.; Bertorelli, R.; Campanella, M.; Nicolussi, E.; Fredduzzi, S.; Reggiani, A. *Eur. J. Neurosci.* **2006**, *23*, 1530.
22. Schuelert, N.; McDougall, J. J. Activation of Cannabinoid CB2 Receptors Reveals a Paradoxical Effect on Joint Pain in Normal and Osteoarthritic Rat Knees; Canada, 2008; Abstract 19C.
23. Evens, N.; Bosier, B.; Lavey, B. J.; Kozłowski, J. A.; Vermaelen, P.; Baudemprez, L.; Busson, R.; Lambert, D. M.; Van Laere, K.; Verbruggen, A. M.; Bormans, G. M. *Nucl. Med. Biol.* **2008**, *35*, 793.
24. Gao, M.; Wang, M.; Miller, K. D.; Hutchins, G. D.; Zheng, Q. H. *Bioorg. Med. Chem.* **2010**, *18*, 2099.
25. Horti, A. G.; Gao, Y.; Ravert, H. T.; Finley, P.; Valentine, H.; Wong, D. F.; Endres, C. J.; Savonenko, A. V.; Dannals, R. F. *Bioorg. Med. Chem.* **2010**, *18*, 5202.
26. Evens, N.; Muccioli, G. G.; Houbrechts, N.; Lambert, D. M.; Verbruggen, A. M.; Van Laere, K.; Bormans, G. M. *Nucl. Med. Biol.* **2009**, *36*, 455.
27. Vandeputte, C.; Evens, N.; Toelen, J.; Deroose, C.; Bosier, B.; Ibrahim, A.; Van der Perren, A.; Gijssbers, R.; Janssen, P.; Lambert, D. M.; Verbruggen, A.; Debyser, Z.; Bormans, G.; Baekelandt, V.; Van Laere, K. *J. Nucl. Med.* **2011**. doi:10.2967/jnumed.110.084426.
28. <<http://www.daylight.com/meetings/emug00/Ertl/tpsa.html>>.
29. Yao, B. B.; Hsieh, G. C.; Frost, J. M.; Fan, Y.; Garrison, T. R.; Daza, A. V.; Grayson, G. K.; Zhu, C. Z.; Pai, M.; Chandran, P.; Salyers, A. K.; Wensink, E. J.; Honore, P.; Sullivan, J. P.; Dart, M. J.; Meyer, M. D. *Br. J. Pharmacol.* **2008**, *153*, 390.
30. Mancini, I.; Brusa, R.; Quadrato, G.; Foglia, C.; Scandroglio, P.; Silverman, L. S.; Tulshian, D.; Reggiani, A.; Beltramo, M. *Br. J. Pharmacol.* **2009**, *158*, 382.
31. Zoghbi, S. S.; Shetty, H. U.; Ichise, M.; Fujita, M.; Imaizumi, M.; Liow, J. S.; Shah, J.; Musachio, J. L.; Pike, V. W.; Innis, R. B. *J. Nucl. Med.* **2006**, *47*, 520.
32. Chitneni, S. K.; Garreau, L.; Cleynhens, B.; Evens, N.; Bex, M.; Vermaelen, P.; Chalon, S.; Busson, R.; Guilloteau, D.; Van Laere, K.; Verbruggen, A.; Bormans, G. *Nucl. Med. Biol.* **2008**, *35*, 75.
33. Muccioli, G. G.; Wouters, J.; Charlier, C.; Scriba, G. K.; Pizza, T.; Di Pace, P.; De Martino, P.; Poppitz, W.; Poupaert, J. H.; Lambert, D. M. *J. Med. Chem.* **2006**, *49*, 872.
34. Fritzberg, A. R.; Whitney, W. P.; Kuni, C. C.; Klingensmith, W., 3rd. *Int. J. Nucl. Med. Biol.* **1982**, *9*, 79.
35. Chitneni, S. K.; Serdons, K.; Evens, N.; Fonge, H.; Celen, S.; Deroose, C. M.; Debyser, Z.; Mortelmans, L.; Verbruggen, A. M.; Bormans, G. M. *J. Chromatogr., A* **2008**, *1189*, 323.
36. Tao, Q.; Abood, M. E. *J. Pharmacol. Exp. Ther.* **1998**, *285*, 651.
37. Casteels, C.; Vermaelen, P.; Nuyts, J.; Van Der Linden, A.; Baekelandt, V.; Mortelmans, L.; Bormans, G.; Van Laere, K. *J. Nucl. Med.* **2006**, *47*, 1858.